OKU Fen Bilimleri Enstitüsü Dergisi
7(5): 2284-2303, 2024

OKU Journal of The Institute of Science and Technology, 7(5): 2284-2303, 2024

Osmaniye Korkut Ata Üniversitesi Fen Bilimleri Enstitüsü Dergisi

Osmaniye Korkut Ata University Journal of The Institute of Science and Technology

Enhancing Aorta Segmentation in Contrast CT Images: A Novel Deep Architectural Approach

Ömer Faruk BOZKIR[1*], Ataberk URFALI[2], Azer CELIKTEN[3], Semih DEMIREL[4], Abdulkadir BUDAK[5], Hakan KARATAS[6], Murat CEYLAN[7]

[1,7]Department of Electrical and Electronics Engineering, Faculty of Engineering and Natural Sciences, Konya Technical University, Konya, Türkiye
[2]Department of Computer Engineering, Faculty of Engineering and Natural Sciences, Konya Technical University, Konya, Türkiye
[3,4,5,6]Akgun Computer Inc., Department of Artificial Intelligence and Image Processing, Ankara, Türkiye

[1]https://orcid.org/0000-0002-3696-3613
[2]https://orcid.org/0000-0001-5709-6718
[3]https://orcid.org/0000-0002-6804-737X
[4]https://orcid.org/0000-0002-3454-3631
[5]https://orcid.org/0000-0002-0328-6783
[6]https://orcid.org/0000-0002-9497-5444
[7]https://orcid.org/0000-0001-6503-9668
*Corresponding author: bozkiromerfaruk@gmail.com

Research Article

Article History:
Received: 23.03.2024
Accepted: 08.07.2024
Published online: 10.12.2024

Keywords:
Aortic segmentation
AKG-UNet
Computer tomography angiography
Deep learning
Image Processing

ABSTRACT

Manual segmentation of patient CT images is both time-consuming and labor-intensive. Additionally, classic image processing techniques are insufficient in CT images due to the close pixel values of tissues. Automatic segmentation of the aorta in human anatomy can reduce healthcare workers' workload in preoperative planning. This study compares the performance of the AKG-Unet segmentation model with other models (U-Net, Inception UNetv2, LinkNet, SegNet, and Res-Unet) on thoracic aorta, abdominal aorta, and iliac arteries segmentation in contrast CT images. Initially, pixel intensities in the Kits and Rider datasets were recalibrated. Then, 2D axial images underwent resizing and grayscale normalization. Segmentation models have been trained and tested with 5-fold cross-validation. 2D prediction masks were stacked to generate a 3D output, and spatial information was transferred to the predicted mask. In the 3B aortic segmentation, small objects adjacent to it were removed using image processing techniques. In our study, the AKG-UNET model achieved the highest segmentation results on the AVT dataset with a Dice score of 91.2%, Intersection-Over-Union (IoU) score of 85.6%, sensitivity of 90.9%, and specificity of 99%. A method has been proposed that helps physicians analyze the aortic structure, and segments the aortic structure so that they can intervene in the correct location and make a preoperative evaluation.

Aort Segmentasyonunu Kontrastlı Bilgisayarlı Tomografi Görüntülerinde Geliştirme: Yenilikçi Derin Mimari Yaklaşımı

Araştırma Makalesi

Makale Tarihçesi:
Geliş tarihi: 23.03.2024
Kabul tarihi:08.07.2024
Online Yayınlanma: 10.12.2024

Anahtar Kelimeler:
Aortik segmentasyon
AKG-UNet
Bilgisayarlı tomografi anjiyografisi
Derin öğrenme

ÖZ

Hasta bilgisayarlı tomografi (BT) görüntülerinin manuel segmentasyonu hem zaman alıcı hem de emek yoğun bir işlemdir. Ayrıca, doku piksel değerlerinin yakınlığı nedeniyle BT görüntülerinde klasik görüntü işleme teknikleri yetersizdir. İnsan anatomisinde aortun otomatik olarak segmentasyonu, ameliyat öncesi planlamada sağlık çalışanlarının iş yükünü azaltabilir. Bu çalışma, kontrastlı BT görüntülerinde torasik aorta, abdominal aorta ve iliak arterlerin segmentasyonunda AKG-Unet segmentasyon modelinin diğer modellerle (U-Net, Inception UNetv2, LinkNet, SegNet ve Res-Unet) performansını karşılaştırır. İlk olarak, Kits ve Rider veri kümelerinde piksel yoğunlukları

Görüntü işleme

yeniden kalibre edildi. Daha sonra, 2B eksenel görüntüler yeniden boyutlandırıldı ve gri tonlaması normalleştirildi. Segmentasyon modelleri 5 katlı çapraz doğrulama yöntemi ile eğitilip test edilmiştir. 2B tahmin maskeleri üst üste eklenilerek 3B bir çıktı elde edildi ve tahmin edilen maskeye mekansal bilgi aktarıldı. 3B aortik segmentasyonun yanındaki küçük nesneler görüntü işleme teknikleri ile kaldırıldı. Çalışmamızda, AKG-UNET modeli, AVT veri setinde Dice skoru %91.2, IoU skoru %85.6, hassasiyet %90.9 ve özgüllük %99 ile en yüksek segmentasyon sonuçlarını elde etti. Doktorların aortik yapıyı analiz etmelerine yardımcı olacak ve doğru konumda müdahale edebilmeleri ve ameliyat öncesi değerlendirme yapabilmeleri için aortik yapının segmentasyonunu yapacak bir yöntem önerilmiştir.

To Cite: Bozkır ÖF., Urfalı A., Celikten A., Demirel S., Budak A., Karatas H., Ceylan M. Enhancing Aorta Segmentation in Contrast CT Images: A Novel Deep Architectural Approach. Osmaniye Korkut Ata Üniversitesi Fen Bilimleri Enstitüsü Dergisi 2024; 7(5): 2284-2303.

1. Introduction

The aorta, the most significant arterial blood channel in the human body, carries blood from the heart to all other organs. Aneurysms, dissections, stenoses, and calcification diseases that occur in the aorta can be detected using 3D medical imaging and if not diagnosed early, can lead to death (Otaki et al., 2020). Therefore, creating a fully automatic system that efficiently and accurately segments the aorta to detect these abnormalities earlier may be advantageous. This procedure is important for understanding the structure and function of the aortic structure and for the diagnosis, preoperative treatment planning, and postoperative monitoring of aortic diseases.

Today, doctors use radiological imaging techniques such as Computer Tomography (CT) and Magnetic Resonance (MR) to examine the body's anatomy, which is displayed in PACS (Picture Archiving and Communication System). Manual vessel analysis in CT images is both difficult and time-consuming for physicians. Additionally, in CT images, 2D-3D segmentation of the anatomical structure is performed using image processing methods such as level-set, fast marching, region growing, and threshold (Lin et al., 2004; Forcadel et al., 2008; Pratondo et al., 2014; Maolood et al., 2018). However, it is difficult to distinguish the vessel and other tissues in contrast-free CT images because the Hounsfield Unit value of the structures is very similar. As a solution to these problems, deep learning-based automatic segmentation studies are conducted.

The initial stage in image analysis is often segmentation. Segmentation is to divide an image into meaningful regions where different features are held (Zhou et al., 2017). In short, tags are created for each pixel and some inferences are made by making predictions about these tags. Image segmentation in medical images is a critical component for preoperative pathology location, treatment planning, and early diagnosis. Manual segmentation in CT scans is expensive for hospitals and time-consuming for physicians. By performing fully automatic segmentation studies in the medical field the workload of physicians is reduced. In recent years, deep learning techniques have been used in face recognition, autonomous vehicles, and the defense industry (Mendi, 2023). Studies on the segmentation of kidney and stones, brain tumors, polyps, blood vessel segmentation in retinal images, liver segmentation, and other organs have been conducted utilizing deep learning approaches in the field of health (Jin et al.,

2018; Bilic et al., 2019; Aldoj et al., 2020; Onthoni et al., 2020; Ter-Sarkisov, 2020; Ranjbarzadeh et al., 2021; Jha et al., 2023).

Many recent studies have also been carried out on aortic segmentation in CT images using deep learning methods.

Dasgupta et al., (2017) proposed an automatic aortic segmentation algorithm of the thorax region, both with and without contrast, from 120 CT images collected from the National Taiwan University Hospital. In this study, Circular Hough Transform (CHT) is applied to determine the localization of the descending and ascending aorta, then active contour is applied to segment the aortic region. They achieved a dice score of 0.88 in the test results.

Zheng et al., (2018) proposed a fully automated method for Abdominal Aortic Aneurysm (AAA) segmentation using little data in their study. They strengthened the data by applying gray value variation and rotation to prevent memorization as a preprocessing. Then they trained the aortic region in the U-Net model to segment it and finally 3D rendered the data obtained as a result of the segmentation. They provided 82.4% Dice Similarity Coefficient (DSC) in the test results.

Noothout et al., (2018) proposed an extended CNN for aortic segmentation with Deep learning methods using 24 low-dose chest CT scans obtained from the National Lung Screening Trial (NLST). In this study, images from three planes were averaged and yielded a dice score of 0.91 in aortic segmentation.

Lareyre et al., (2019) proposed a method for detecting Vascular and AAA. In their study, they performed it in four steps using 40 CT scan data. In the first step, they applied window/level and noise reduction as preprocessing. In the second step, they performed the segmentation of the aortic lumen by determining a contour with the threshold-based method. Finally, they performed segmentation of thrombus and segmentation of calcifications using lumen segmentation. In the test results, the mean sensitivity for segmentation of the aortic lumen was 0.90 +/ 0.06, the mean specificity was 0.9997 +/ 0.0004, the mean Jaccard index was 0.87 +/ 0.07; they provided an average DSC of 0.93 +/ 0.04.

Morris et al., (2020) proposed a segmentation method with a 3D U-Net model using CT and MR images to segment the heart. In the study, they provided a 0.85 dice score in aortic segmentation.

Fantazzini et al., (2020) proposed a deep learning approach for a spatially compatible segmentation of the thoracic aorta, abdominal aorta, and iliac arteries in their study. First, they performed segmentation with 2D U-Net in axial view to determine the localization of the aorta. They divided the localized aorta into axial, coronal, and sagittal planes and performed resizing, data augmentation (rotation, width shift, height shift), and set the window level and width on the images to 800-200, respectively, as preprocessing. During the training phase, axial, coronal, and sagittal data were trained with three separate U-Net architectures. Finally, they rendered the resulting 2D three segmentation regions in 3D. In their test results, they achieved a DSC of 0.92 ± 0.01.

Bonechi et al., (2021) in their study, proposed a fully automatic method for segmentation of the abdominal aorta. They presented an automated method for segmentation of the aorta based on 2D CNN using 3D CT scans as input. In the study, they used a dataset consisting of 153 CT images. They analyzed

it using three 2D segmentation meshes, one for each of the axial, sagittal, and coronal planes in the image scan. In the study, they compared two different network architectures, U-Net and LinkNet, by applying ResNet V2 and ResNet34 architectures as backbones. In this study, they applied cropping and adaptive histogram equalization to image dimensions as preprocessing. As a result of the training, they showed that the LinkNet+ResNetV2 model gave the best result. In the test results for the three planes, they obtained an axial 83.45%, coronal 77.11%, and sagittal 76.75% IoU Score.

Wang et al., (2022) proposed a two-stage deep learning method consisting of contrast enhancement and segmentation model to overcome the difficulty in segmentation of non-contrast CT images of the aorta and pulmonary arteries. They used the contrast enhancement model to increase the success of segmentation of the aorta and pulmonary arteries. Applying five-fold cross-validation in training, they obtained Dice coefficients of 0.97 ± 0.66 and 0.93 ± 0.16 in the segmentation results of the aorta and pulmonary artery, respectively.

In their study, researchers presented an approach to improve the performance of aortic segmentation in 18 CT scans (Benčevi´benčevi´c et al., 2022). In the study, as a preprocess, the image dimensions were 256×256, the window range of CT scans was 200-500 HU, and they performed normalization on the data in the range of [-0.5,0.5]. Data augmentation methods were applied to these obtained data. They first roughly segmented the training-ready axial data in the U-Net model. The segmentation data they obtained were passed through polar transform networks separately by determining the center points for each object. They inverted the weighted pole estimates they obtained as a result of the network and combined them into a single image. Finally, they performed aortic segmentation by setting a threshold of 0.4. As a result, they obtained a 0.932 ± 0.027 Dice score and 0.895 ± 0.033 mIoU score in aortic segmentation.

Brutti et al. (2022) proposed a method for automatic partitioning of intraluminal thrombi within the aorta and subsequent analysis of abdominal aortic aneurysm (AAA) geometry using CT angiography (CTA) images. The dataset used in their study comprised 85 CTA scans provided by IRCCS Ospedale Policlinico San Martino (Genoa, Italy). They performed lumen segmentation using a U-Net model and, for thrombus segmentation, they initially localized the aortic structure in three separate planes using a U-Net model and then conducted the segmentation process. The obtained results yielded a Dice score of 0.89 ± 0.04 for thrombus segmentation.

In this study, deep learning algorithms were used to segment the aortic structure extending from the left ventricle to the abdominal region in contrast to CT image scans, and 3D visualization was performed. The study aims to achieve full automatic segmentation of the thoracic aorta, abdominal aorta, and iliac arteries. This will enable 3D analysis of the aortic lumen and assist doctors in preoperative planning and periodic follow-up.

It has been observed that models in the literature are inadequate for aortic segmentation and particularly for segmenting small objects. To address this issue, the AKG-Module was developed, leading to the

creation of the novel AKG-Unet model. AKG-Unet not only improves performance but also significantly reduces computational cost.

The high number of parameters in existing models, the need for training separate models for each plane, and the use of 3D CNN structures prolong both training and prediction times. To overcome these challenges, AKG-Unet integrates Depth-Wise and SE blocks. These blocks enhance the model's efficiency by reducing the number of parameters while improving performance.

The unique architecture of AKG-Unet is notable for its ability to simultaneously extract both low-level and high-level features. In the encoder section, the use of 7×7 depthwise separable convolutions and SE blocks optimizes performance and increases efficiency. These features ensure that AKG-Unet maintains its efficiency even when working with large datasets and high-resolution images.

In conclusion, AKG-Unet has the capacity to create more complex structures and produce more precise results compared to traditional U-Net and Inception U-Net models. These characteristics make AKG-Unet a reliable model that demonstrates superior performance, particularly with complex and detailed image data.

The main contributions of this study are presented below:

• We took advantage of a brand-new dataset of contrast CT imaging scans from, published in 2022 (Radl et al., 2022).

• A new AKG-UNet segmentation network was designed to improve the success of aortic segmentation.

• In the new dataset, the AKG-UNet, U-Net, Inception U-Netv2, LinkNet, SegNet and Res-UNet segmentation algorithms were tested, and the results are presented comparatively (Ronneberger et al., 2015; Badrinarayanan et al., 2017; Chaurasia et al., 2017; Delibasoglu et al., 2020; Diakogiannis et al., 2020; Urfali et al., 2023).

• Results were obtained with a 2D Convolutional Neural Network (CNN) using axial images. Afterward, 3D segmentation results were visualized with the Medical Imaging Interaction Toolkit (MITK) interface program and post-preprocessing methods.

The remaining parts of this article are organized as follows. In the second part, related studies are given. In the second part, the data set used, the methods followed, the newly designed AKG-UNet model used in the study and finally the performance criteria are explained. In Chapter 3, the results of the study are compared and presented. In Chapter 4, the result of the study is explained briefly and concisely.

2. Material and Method

In this section, the dataset is explained in detail in section 2.1. In Section 2.2, preprocessing done on the dataset is explained. The system architecture is explained in detail in Section 2.3. In Section 2.4, the designed AKG module and AKG-Unet structure are explained. Section 2.5 describes the performance criteria used in the study to compare the models.

2.1. Dataset

The AVT dataset consists of the combination of Dongyang Kits Rider datasets, and this dataset was published by Radl et al. (2022). The AVT dataset was also used our study. This dataset comprises contrast-enhanced scans of the aorta and its branches, including the thoracic aorta, abdominal aorta, and iliac artery, specifically designed for segmentation in deep learning algorithms. As seen in Table 1, information for the Dongyang, Kits, and Rider datasets is provided. In this study, a total of 22,753 axial sections from 56 CT scans were utilized across the Dongyang, Kits, and RIDER datasets. The RIDER dataset encompasses not only normal image scans but also includes pathologies such as AAA and Aortic Dissection.

Table 1. Dataset properties (Yuan et al., 2023).

Image Information	DONGYANG	KITS	RIDER
Image Size	512×666	512×512	512×512
Number of Axial Scans	2840	5394	14519
Number of Cases	18	20	18
Slice thickness	2/3/3 mm	0.5/5/5 mm	0.625/0.625/2.5 mm
Pathologies	None	None	AD, AAA

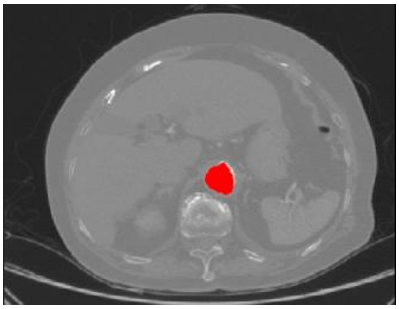

(a)

(b)

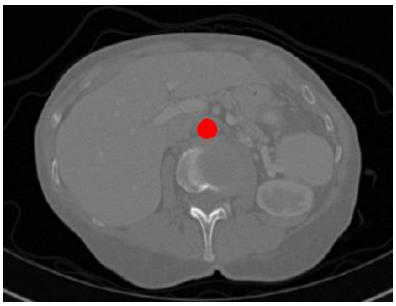

(c)

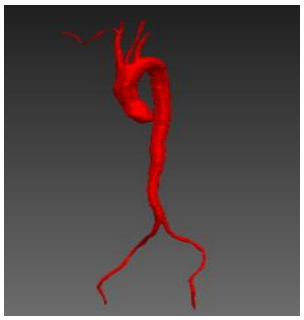

(d)

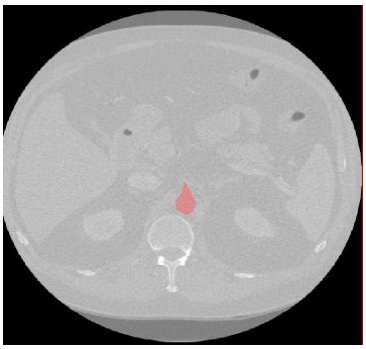

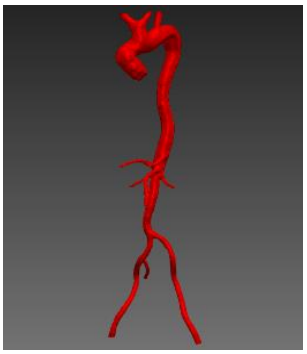

(e) (f)

Figure 1. 2D images and 3D ground truth masks from different dataset (Radl et al., 2022) (a) 2D axial view in Dongyang dataset, (b) 3D axial view in Dongyang dataset, (c) 2D axial view in Kits dataset, (d) 3D axial view in Kits dataset, (e) 2D axial view in Rider dataset, (f) 3D axial view in Rider dataset

2.2. Preprocessing

To successfully train deep learning networks, data preprocessing is essential. Below, all the steps related to data preprocessing are explained in order.

• In axial slices in the Dongyang, Kits, and Rider datasets, 512×666 and 512×512 image sizes were resized to 256×256.

• The central intensities of the aorta, which are clinically significant in the Kits and Rider datasets, are approximately 1024 units higher compared to the D dataset. This pixel difference may lead to the inability to obtain HU values in the same range across all datasets, potentially causing a decrease in training success. Therefore, we adjusted all pixel values in the Kits and Rider datasets by reducing them by 1024 units (Yuan et al., 2023).

• The HU range in the Dongyang, Kits, and Rider datasets were set to 200-500.

• 0-1 grayscale normalization process was applied to the images.

2.3. Aortic Segmentation

The recommended approach for 3D segmentation of the aorta from 2D CT scans is as shown in Figure 2. As seen in the system architecture, the contrasted images are first preprocessed. After preprocessing, the data were trained with AKG-UNet, U-Net, Inception U-Netv2, LinkNet, SegNet, and Res-UNet models. At the end of the training, the test process was carried out and the obtained axial mask images were converted to nii format by overlapping. The location header information of the original image series was transferred to the resulting 3D prediction masks. By applying the method of removing small-area objects on the predicted series, the false negative objects that were segmented around the vessel as a result of prediction were cleaned and improved. 3D prediction masks were visualized in 3D in the MITK application (MITK-Diffusion, 2023). Finally, the 3D prediction masks obtained from AKG-UNet, U-Net, Inception U-Netv2, LinkNet, SegNet and Res-Unet were compared using performance metrics.

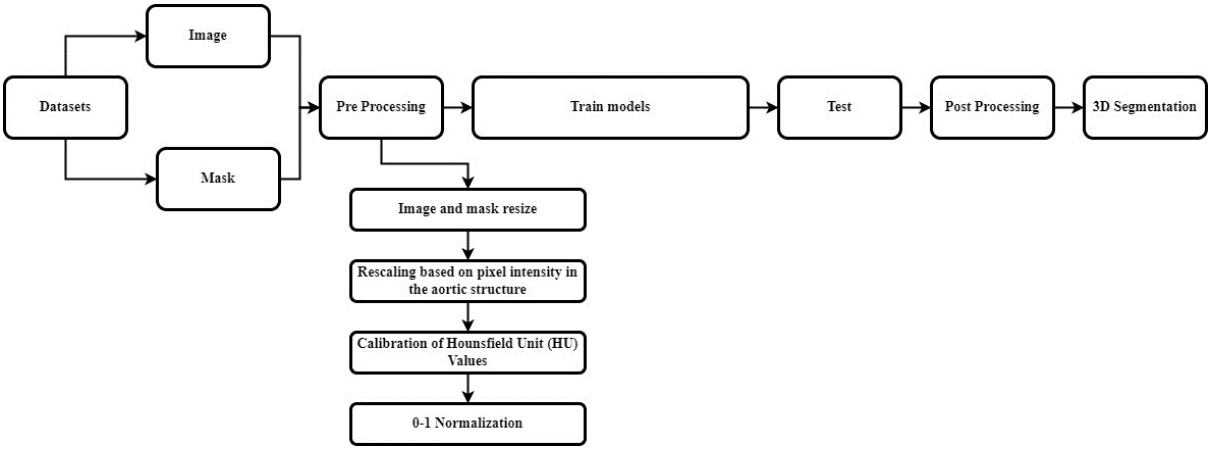

Figure 2. System architecture

2.4. AKG-Unet

When compared to the conventional U-Net and Inception U-Net, AKG-Unet exhibits a distinct architectural design, as seen in Figure 3. This differentiation is most pronounced in the configuration of the encoder section. The principal departure from Inception U-Net lies in the incorporation of specialized components referred to as the "AKG Module" within the encoder module of AKG-Unet (Urfali et al., 2023). A notable innovation introduced by this unique module is its capacity to amalgamate filters of varying dimensions. The distinctive architecture of AKG-Unet not only enhances performance but also reduces computational costs and power consumption. This advantage becomes particularly prominent when juxtaposed with similar models such as Inception U-Net and the conventional U-Net. Notably, the utilization of the AKG Module enables the construction of more intricate structures while necessitating fewer input parameters. Consequently, the model operates at an accelerated pace and requires less memory. AKG-Unet maintains its operational efficiency even when processing extensive datasets and high-resolution images, thanks to reduced computational overhead. The encoder section plays a pivotal role in data processing and feature extraction. Unlike the conventional U-Net, AKG-Unet employs a unique approach in its encoder component. It commences with the conventional 3×3 binary convolution process as the initial step in the extraction of crucial information. Subsequently, the AKG Module is seamlessly integrated, facilitating the model's efficient construction of increasingly intricate structures. This integration enhances the network's ability to accurately represent data, resulting in more precise outcomes. In contrast to the conventional U-Net architecture, the decoder section of AKG-Unet adopts a different strategy. While traditional U-Net models frequently employ binary 3×3 convolutions, we opt for the more efficient "depthwise separable convolutions" in the decoder section (Chollet, 2017). This preference is founded upon a fundamental principle in U-Net architecture: essential features are extracted in the encoder section and subsequently relayed to the decoder section. Depthwise separable convolutions effectively reduce the number of parameters, eliminating the need for superfluous weights

and diminishing pixel-level dependencies. Consequently, a lighter and more computationally efficient model is achieved. In the case of AKG-Unet's decoder section, the objective is not only parameter reduction but also the preservation of performance. Compared to conventional convolutions, depthwise separable convolutions can achieve similar performance with fewer parameters. This translates to reduced computational costs, expedited training, and swifter results. The incorporation of the AKG Module within the framework of AKG-Unet equips it with the capability to express more intricate features, constituting a significant advantage. This attribute contributes to the model's capacity to produce more accurate results. AKG-Unet exhibits the potential to yield superior outcomes compared to conventional U-Net and Inception U-Net models, particularly when dealing with complex and detailed image data. The unique encoder design of AKG-Unet empowers the model to efficiently generate more intricate structures, culminating in outcomes that are notably precise and accurate.

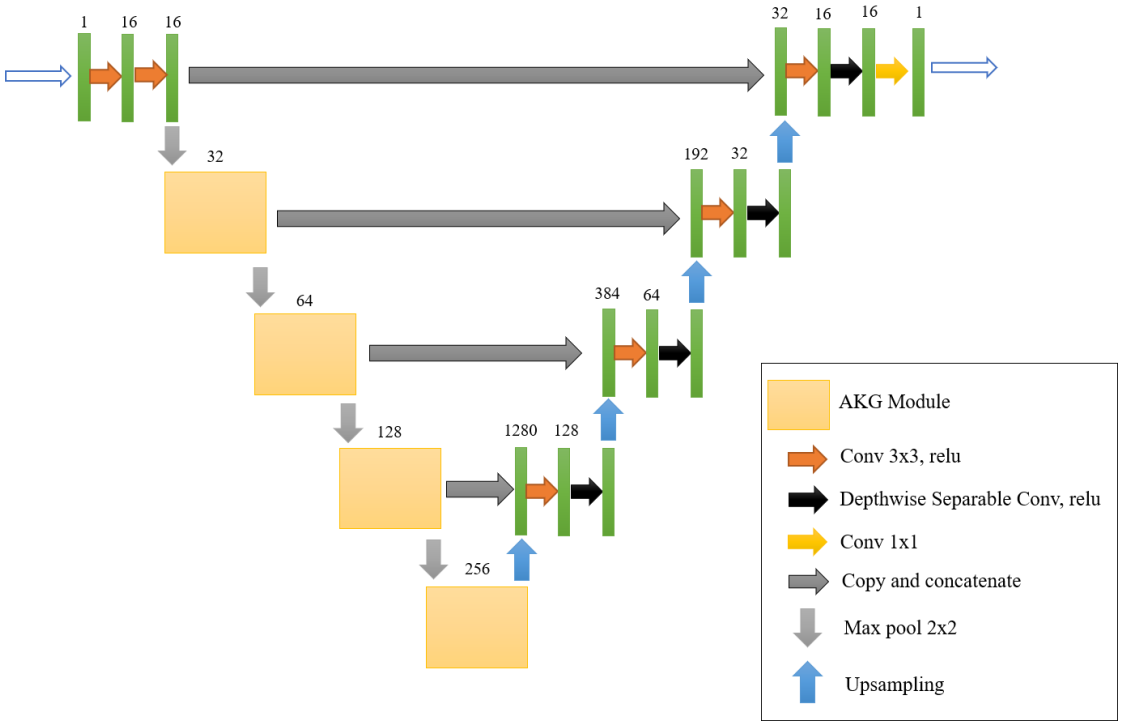

Figure 3. AKG-Unet architecture (Urfali et al., 2023)

2.4.1. AKG-Module

Since GoogleNet initially made the "Inception module" available, it has grown significantly in prominence, especially for issues with medical image processing (Szegedy et al., 2015). This section aims to provide a technical explanation of the fundamental functionality of the module, referred to as the "AKG-Module" as illustrated in Figure 4 (Urfali et al., 2023). The Inception module is exceptional in that it can concurrently extract both low-level and high-level characteristics. With this capacity, feature quality is improved, variety is increased, and better outcomes are possible. The Inception module produced outstanding results even in its early iterations, and it has since been enhanced in subsequent research. To increase the effectiveness of the Inception module, several changes have been added. These

improvements attempt to decrease the amount of parameters while enhancing the performance of the module. The Inception module of the AKG module now has 7×7 size depthwise separable chunks. This decreases the amount of parameters while improving the performance of the module. After the module, SE blocks were added, which improved performance while spending less on computation (Hu et al., 2023). Similar to attention processes, SE blocks function by highlighting critical characteristics and suppressing less significant ones.

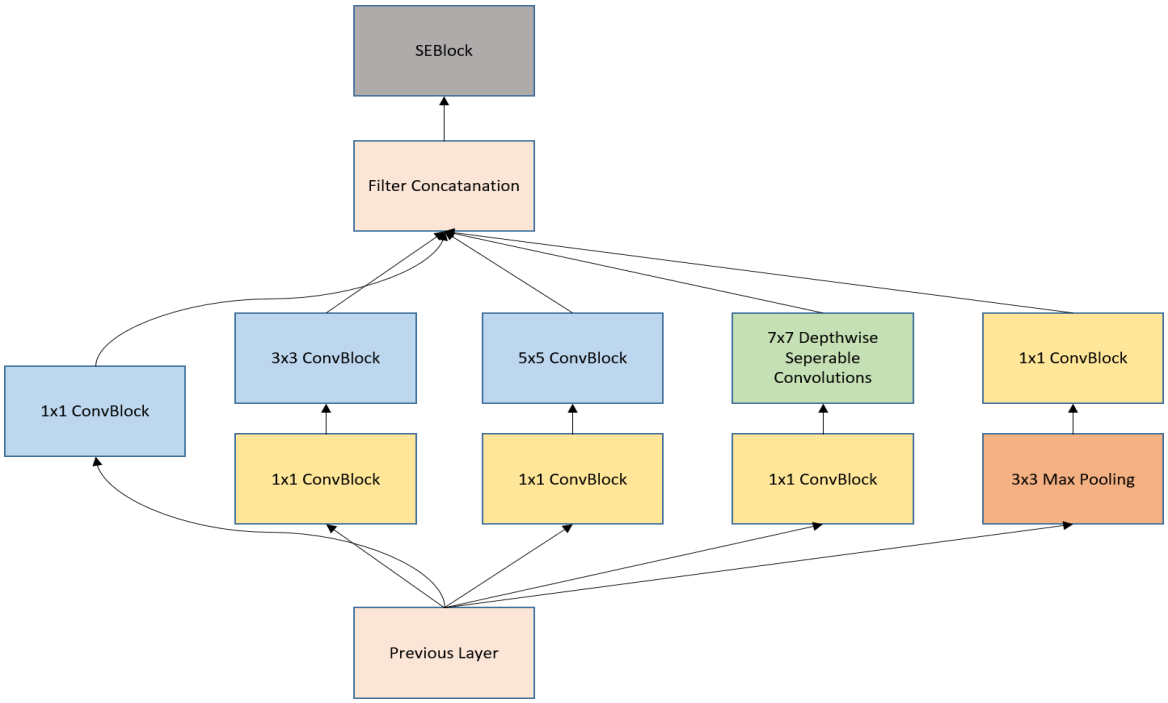

Figure 4. AKG-MODULE architecture (Urfali et al., 2023)

2.5. Performance Metrics

In deep learning studies, metrics are used to measure the performance of the model and to compare different models. In this study, four different pixel-based performance measures, namely Sensitivity, Specificity, Dice, and IoU, were calculated to compare success measures in AKG-UNet, U-Net, Inception U-Net, LinkNet, SegNet, and Res-Unet models. The Confusion Matrix is a matrix model that gives information about the classification performance over the real and predicted images on the data. As seen in Table 2, the columns represent the estimation of positive and negative, rows the actual positive and negative. By using the values in this matrix, the calculations of Sensitivity, Specificity, Dice, and IoU metrics were made.

- TP: Examples where the true value is 1 (True) and the estimated value is 1 (Positive).
- FN: Examples where the actual value is 1 (True) but the estimated value is 0 (Negative).
- FP: Examples where the true value is 0 (False) but the predicted value is 1 (Positive).
- TN: Examples where the true value is 0 (False) and the predicted value is 0 (Negative).

2.5.1. Sensitivity

Sensitivity, as shown in equation 1, expresses the ratio with which the pixels that need to be segmented in the image during a segmentation process can be detected.

$$Sensitivity = \frac{TP}{TP + FN} \quad (1)$$

2.5.2. Specificity

Specificity, as seen in equation 2, expresses the ratio at which the pixels that should not be segmented on a pixel basis in a segmentation process can be detected.

$$Specificity = \frac{TN}{TN + FP} \quad (2)$$

2.5.3. Dice score

Dice score is a pixel-based performance measure used especially in health studies. It is calculated as shown in equation 3.

$$Dice = \frac{2 * TP}{2 * TP + FN + FP} \quad (3)$$

2.5.4. Intersection-Over-Union (IoU, Jaccard Index)

The Jaccard Index, often known as Intersection over Union (IoU), is one of the most popular metrics in semantic segmentation. It is calculated as seen in Equation 4. This metric is also associated with the Dice calculation.

$$IoU = \frac{TP}{TP + FP + TN} \quad (4)$$

3. Results and Discussion

This experimental study was performed using 56 contrast-enhanced CT image scans from three different datasets. Training, validation, and testing were performed under the Windows 10 operating system, using Intel(R) Core (TM) i7-10700 CPU @ 2.90 GHz processor, 16.0 GB Memory, and NVIDIA® GeForce RTX 3060 12GB graphics card. Python software language was used in the whole process of the study. Anaconda's Spyder ide was used during the training and testing process. In this study, our designed AKG-UNet model was compared with U-Net, Inception U-Netv2, LinkNet, SegNet and Res-Unet models, and the Cross Entropy + Dice loss was employed as the hyperparameter during the training process. The learning rate of the models was set to 0.001, batch size 2, and epoch number 50. Root Mean Square Propagation (RMSprop) was used as the optimization algorithm to minimize the overall error and loss function. 10% of the data was set aside for testing. The remaining 90% was used for training

with 5-fold cross-validation. The 2D images obtained at the end of the test process were combined and turned into 3D in NIfTI format. Two processes were carried out as post-processing. In the first of these, although the 2D estimated masks were detected close to the truth, distortion was detected in the 3D images, as seen in Figure 5a, due to the lack of coordinate information of the 3D scan created. This problem was solved by automatically transferring the coordinate information in the original image to the estimated mask scan with the Python code, as seen in Figure 5b. Finally, the false negative regions in the 3D images as a result of the segmentation were removed with the remove small object function of the skimage library, as seen in Figure 6, and the images 6a and 6b have been cleaned and the 3D images improved, as seen in 6c and 6d.

(a) (b)

Figure 5. Applying original image metadata onto the predicted masks. (a) 3D image obtained as a result of the test, (b) 3D image with location information transferred from original scan to estimated scan.

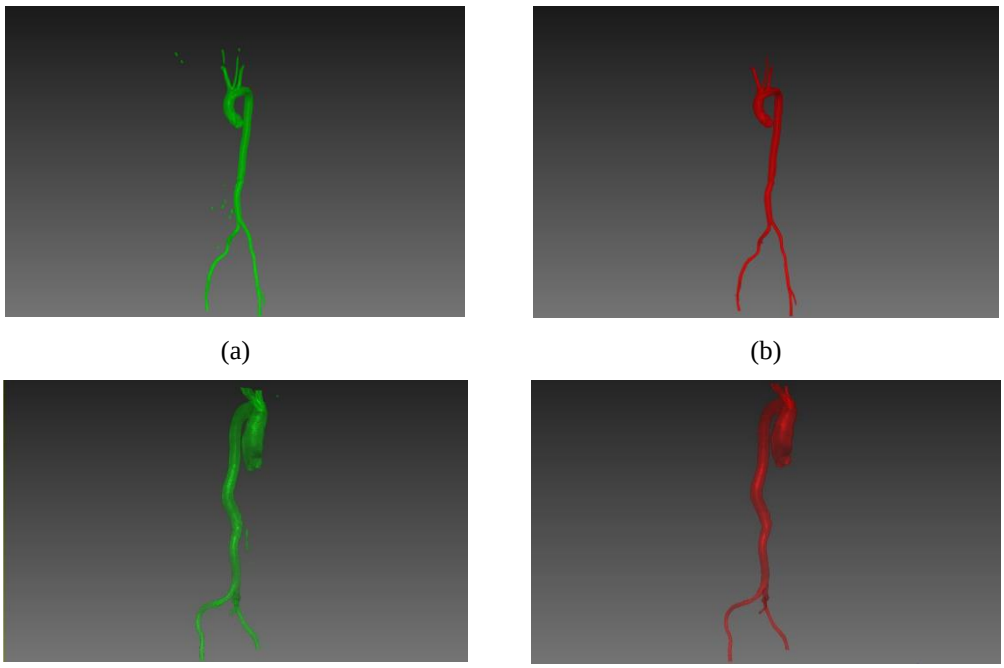

(a) (b)

(c) (d)

Figure 6. Reducing false positives in predicted 3D masks. (a) and (c) Show the predicted mask, (b) and (d) Remove Small Object

In this study, the test results obtained by combining DONGYANG, KITS, and RIDER data of LinkNet, SegNet, ResUnet, U-Net, Inception U-Netv2, and AKG-UNet models trained on 2D axial images with 5-fold Cross Validation are compared in Table 3. In LinkNet, 87.2% Dice, 77.4% IoU, %82.9 sensitivity, and 99.9% specificity was obtained, 84.9% Dice, 74.0% IoU, 79.3% sensitivity, 99.9% specificity were obtained in SegNet, and 87.5% Dice, 78.1% IoU, 83.1% sensitivity, 99.9% specificity were obtained in ResUNet, and 90.2% Dice, 82.2% IoU, 87.6% sensitivity, 99.9% specificity were obtained in U-Net, and 90.9% Dice, 83.3% IoU, 88.8% sensitivity, 99.9% specificity were obtained in Inception U-Netv2, and 91.2% Dice, 85.6% IoU, 90.0% sensitivity, 99.9% specificity were obtained in AKG-UNet. In the training results obtained by combining the Dongyang, KITS, and RIDER datasets, it was seen that the AKG-UNet model gave higher results than the other models. Figure 7 shows the 2D axial results obtained by U-Net, Inception U-Netv2, LinkNet, SegNet, Res-Unet, and AKG-UNet models, respectively. Finally, the 3D segmentation results of the models are shown as shown in Figure 8.

Table 3. Dongyang, Kits and Rıder datasets test results by applying 5-Fold Cross-validation on LinkNet, SegNet and Res-Unet, Inception U-Netv2, U-Net, AKG-UNet models

DONGYANG+KITS+RIDER (Yuan et al., 2023)	DICE	IOU	SENS	SPE	MODEL PARAMETER(M)	Weight Files(MB)
LinkNet	0.872	0.774	0.829	0.999	11,527,234	44
SegNet	0.849	0.740	0.793	0.999	29,443,010	112
ResUNet	0.875	0.781	0.831	0.999	13,040,770	49.8
U-Net	0.902	0.822	0.876	0.999	31,036,546	124.2
Inception U-Netv2	0.909	0.833	0.888	0.999	32,041,850	125.3
AKG-UNet	0.912	0.856	0.900	0.999	10,413,408	40.8

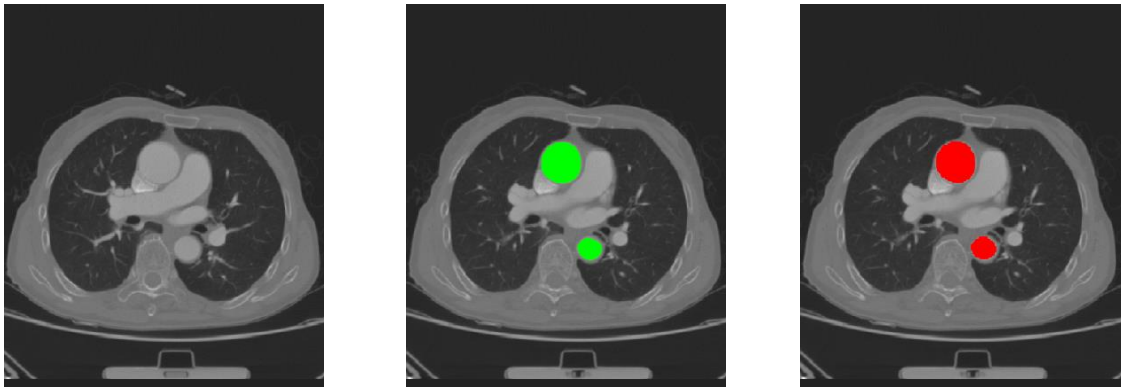

(a) (b) (c)

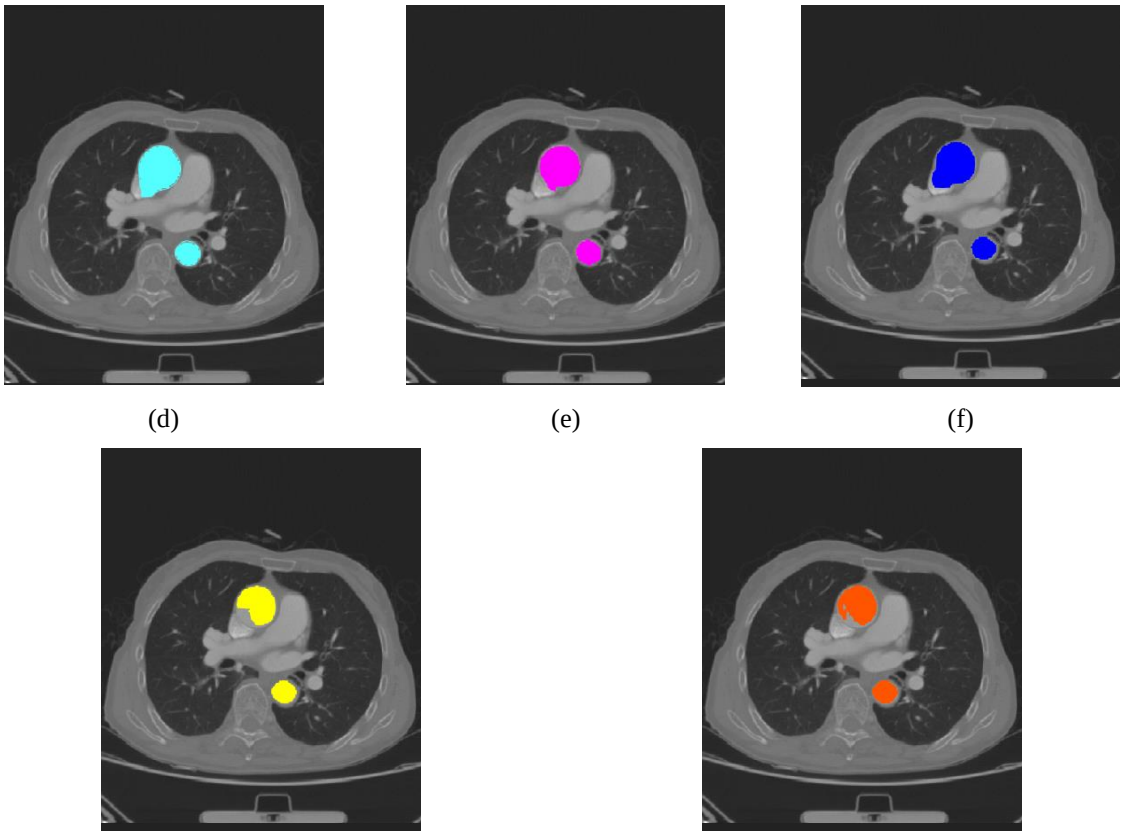

(d) (e) (f)

(g) (h)

Figure 7. Segmentation results of the aorta in 2D axial slices. (a) Input test image, (b) ground truth mask of the input test image, (c) Predicted mask by using AKG-Unet on the test image, (d) Predicted mask by using Inception U-Netv2 on the test image, (e) Predicted mask by using U-Net on the test image, (f) Predicted mask by using ResUnet on the test image, (g) Predicted mask by using LinkNet on the test image, (h) Predicted mask by using SegNet on the test image

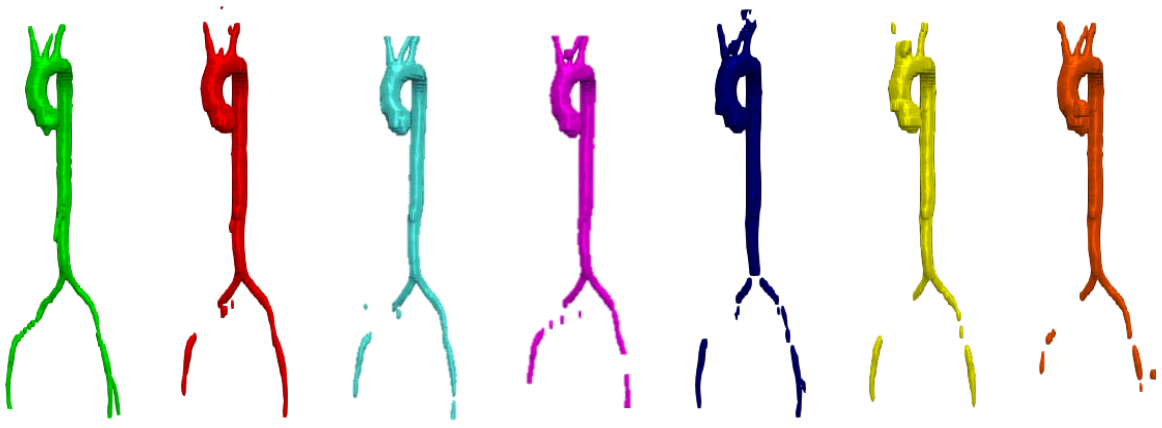

(a) (b) (c) (d) (e) (f) (g)

Figure 8. 3D test results of aort segmentation (a) ground truth, (b) 3D prediction result obtained by AKG-UNet, (c) 3D prediction result obtained by Inception U-Netv2, (d) 3D prediction result obtained by U-Net, (e) 3D prediction result obtained by ResUNet, (f) 3D prediction result obtained by LinkNet, (g) 3D prediction result obtained by SegNet

The performance criteria of this study with the aortic studies conducted in the literature are compared in Table 4.

Table 4. Comparison of the results with previous studies for Aort segmentation

Study	DATASET	CASE	DICE	IOU	SEN	SPE
Dasgupta et al. (2017)	LIDC-IDRI	30	0.880	X	X	X
Zheng et al. (2018)	PRIVATE	-	0.824	X	X	X
Noothout et al. (2018)	PRIVATE	24	0.910	X	X	X
Lareyre et al. (2019)	PRIVATE	40	0.930	0.870	0.900	0.999
Morris et al. (2020)	PRIVATE	25	0.850	X	X	X
Fantazzini et al. (2020)	PRIVATE	80	0.928 ± 0.013	0.866 ± 0.023	X	X
Bonechi et al. (2021)	PRIVATE	153	X	0.835	X	X
Wang et al. (2022)	PRIVATE	179	0.970	X	X	X
Benčevi´benčevi´c et al. (U-Net) (2022)	AVT (Dongyang)	18	0.886± 0.049	X	X	X
Brutti et al. (2022)	PRIVATE	85	0.89 ± 0.04	X	X	X
Our Study (LinkNet)	AVT	**56**	**0.872**	**0.774**	**0.829**	**0.999**
Our Study (SegNet)	AVT	**56**	**0.849**	**0.740**	**0.793**	**0.999**
Our Study (ResUNet)	AVT	**56**	**0.875**	**0.781**	**0.831**	**0.999**
Our Study (U-Net)	AVT	**56**	**0.902**	**0.822**	**0.876**	**0.999**
Our Study (Inception U-Netv2)	AVT	**56**	**0.909**	**0.833**	**0.888**	**0.999**
Our Study (AKG-UNet)	AVT	**56**	**0.912**	**0.856**	**0.900**	**0.999**

When the results of aortic segmentation were compared with previous studies, it was seen that significant results were obtained and more successful results were obtained than many studies in the literature.

Dasgupta et al. (2017) first applied a Circular Hough Transform (CHT) to localize the aorta, then active contouring to segment the aorta. However, it was observed in our study that the deep learning models U-Net, Inception U-Netv2, and the model we designed, AKG-UNet, provided higher dice scores.

In the study by Zheng et al. (2018), the network was trained for axial images using a 2D CNN network. Afterwards, 3D outputs were obtained by following a 3D reconstruction method similar to the method applied by us. However, when we look at the Dice Score obtained, it is observed that the Dice Score obtained by us is higher among the six models.

In the study conducted by Noothout et al. (2018), a segmentation study related to the iliac arteries was not performed while conducting aortic segmentation. Due to the small size of the iliac arteries, there is a decrease in segmentation success in this context. Taking these factors into account, we conducted a more comprehensive analysis in our study, and additionally, the AKG-UNet model yielded a higher Dice Score.

In the studies carried out by Bonechi et. al. (2021) and Fantazzini et. al. (2020) the images were given as input to three different networks for axial, sagittal and coronal images using 2D CNN network. Afterwards, the obtained predictions were rendered in 3D. This extends the prediction time in addition to the training time of the model. In the study carried out by us, the training and estimation process of the model was completed with a single axial view. Afterwards, 3D outputs were obtained through the MITK intermediate program. Additionally, our designed AKG-UNet model achieved a higher IoU score compared to the study conducted by Bonechi et al. (2020).

Morris et al. (2020) performed segmentation with a 3D U-Net model to segment the heart. A higher dice scores were achieved compared to Morris et al.'s work, except for the SegNet model. In addition, in our study, 2D LinkNet, SegNet, ResUNet and AKG-UNet models can be used instead of 3D U-NET to produce faster estimation result with fewer parameters.

Although Wang et al.'s (2022) performance rates were higher than our study, the size of the dataset they used was also larger than ours. The point where we differ from this work is the 3D visualization.

In their study, Buritti et al. (2022) performed aortic lumen and thrombus segmentation to conduct diameter analysis for AAA. Despite utilizing a larger amount of CTA data in their study, our research attained a higher Dice score in the deep learning models, including U-Net, Inception U-Netv2, and our custom-designed AKG-UNet.

In the study by Benčevi´benčevi´c et al. (2022), aortic segmentation was performed by training on the CT dataset collected from the DONGYANG hospital, which was also used in our study, using U-Net and polar transform networks. In our study, to increase data diversity and conduct a more comprehensive analysis, training was conducted using the DONGYANG, KITS, and RIDER datasets. As a result, a higher Dice score was attained in the U-Net, Inception U-Netv2, and our designed AKG-UNet models. In the studies to be carried out after this stage, our aim is to make improvements on the aortic anatomy performance and to determine the regions such as aneurysm and vasoconstriction in a fully automatic manner by calculating the diameter and area of the segmented aortic vessel.

4. Conclusion

In this study, a deep learning approach is proposed for the segmentation of the thoracic aorta, abdominal aorta, and iliac arteries in contrast to CT scans. In the proposed System architecture design, firstly, axial CT data were preprocessed, then by training and testing of U-Net, Inception U-Netv2, LinkNet, SegNet, ResUNet, and AKG-UNet models, 2D estimated mask sections have been created, and these 2D sections have been combined on top of each other. By removing small objects and adding coordinate information from the original image to the 3D radiological image obtained, the distortions in the 3D view were corrected and displayed in 3D in the MITK interface. As a result, in the aortic segmentation study, the best performance criterion was achieved in the AKG-UNet model that we designed. In the AKG-UNet model, we obtained scores of 91.2% for Dice, 85.6% for IoU, 90.0% for sensitivity, and 99.9% for specificity. Additionally, this study contributes to the literature with the introduction of the AKG-UNet model. As a result of this study, a system has been developed that uses aortic segmentation to significantly reduce the workload of surgeons during the preoperative planning and follow-up stages of treatment for conditions such as aneurysms and vascular narrowing, and make decision-making easier. In future works, virtual reality applications may be used with the proposed system. Virtual reality technologies have been widely used in the health sector in recent years. Following this, this study aims to help physicians examine the aorta structure as close to reality as possible in vascular analysis through

the integration of 3D segmentation of the aortic structure into virtual reality applications. Finally, the system is promising in clinical applications and is open to development.

Acknowledgements

This paper has been prepared by AKGUN Computer Incorporated Company. We would like to thank AKGUN Computer Inc. for providing all kinds of opportunities and funds for the execution of this project.

Statement of Conflict of Interest

The authors have no conflicts of interest to declare.

References

Aldoj N., Biavati F., Michallek F., Stober S., Dewey M. Automatic prostate and prostate zones segmentation of magnetic resonance images using densenet-like u-net. Scientific Reports 2020; 10(1): 1-17.

Badrinarayanan V., Kendall A., Cipolla R. Segnet: a deep convolutional encoder-decoder architecture for ımage segmentation. IEEE Transactions on Pattern Analysis and Machine Intelligence 2017; 39(12): 2481-2495.

Benčevi´benčevi´c M., Habijan M., Gali´cgali´c I., Babin D. Using the polar transform for efficient deep learning-based aorta segmentation in cta ımages. International Symposium Elmar 2022 Sep 12, pp. 191-194.

Bilic P., Christ P., Li HB., Vorontsov E., Ben-Cohen A., Kaissis G., Szeskin A., Jacobs C., Mamani GEH., Chartrand G., Lohöfer F., Holch JW., Sommer W., Hofmann F., Hostettler A., Lev-Cohain N., Drozdzal M., Amitai MM., Vivanti R., Sosna J., Ezhov I., Sekuboyina A., Navarro F., Kofler F., Paetzold JC., Shit S., Hu X., Lipková J., Rempfler M., Piraud M., Kirschke J., Wiestler B., Zhang Z., Hülsemeyer C., Beetz M., Ettlinger F., Antonelli M., Bae W., Bellver M., Bi L., Chen H., Chlebus G., Dam EB., Dou Q., Fu CW., Georgescu B., Giró-I-Nieto X., Gruen F., Han X., Heng PA., Hesser J., Moltz JH., Igel C., Isensee F., Jäger P., Jia F., Kaluva KC., Khened M., Kim I., Kim JH., Kim S., Kohl S., Konopczynski T., Kori A., Krishnamurthi G., Li F., Li H., Li J., Li X., Lowengrub J., Ma J., Maier-Hein K., Maninis KK., Meine H., Merhof D., Pai A., Perslev M., Petersen J., Pont-Tuset J., Qi J., Qi X., Rippel O., Roth K., Sarasua I., Schenk A., Shen Z., Torres J., Wachinger C., Wang C., Weninger L., Wu J., Xu D., Yang X., Yu SC., Yuan Y., Yue M., Zhang L., Cardoso J., Bakas S., Braren R., Heinemann V., Pal C., Tang A., Kadoury S., Soler L., van Ginneken B., Greenspan H., Joskowicz L., Menze B. The liver tumor segmentation benchmark (lits). Medical Image Analysis 2023; 84: 102680.

Bonechi S., Andreini P., Mecocci A., Giannelli N., Scarselli F., Neri E., Bianchini M., Dimitri GM. Segmentation of aorta 3d ct images based on 2d convolutional neural networks. Electronics 2021; 10(20): 2559.

Brutti F., Fantazzini A., Finotello A., Müller LO., Auricchio F., Pane B., Spinella G., Conti M. Deep learning to automatically segment and analyze abdominal aortic aneurysm from computed tomography angiography. Springer 2022;13(4):535-547.

Chaurasia A., Culurciello E. Linknet: Exploiting encoder representations for efficient semantic segmentation 2017 IEEE Visual Communications and Image Processing, 1-4 January 2018.

Chollet F. Xception: deep learning with depthwise separable convolutions. In Proceedings of the IEEE Conference on Computer Vision and Pattern Recognition 2017: 1251-1258.

Dasgupta A., Mukhopadhyay S., Mehre SA., Bhattacharyya P. Morphological geodesic active contour based automatic aorta segmentation in thoracic ct images. Proceedings of International Conference on Computer Vision and Image Processing - CVIP 2016, Indian Institute of Technology Roorkee, 26-28 February 2016:187-195.

Delibasoglu I., Cetin M. Improved u-nets with inception blocks for building detection. JARS 2020; 14(4): 044512.

Diakogiannis FI., Waldner F., Caccetta P., Wu C. Resunet-a: a deep learning framework for semantic segmentation of remotely sensed data. ISPRS Journal of Photogrammetry and Remote Sensing 2020; 162: 94-114.

Fantazzini A., Esposito M., Finotello A., Auricchio F., Pane B., Basso C., Spinella G., Conti M. 3d automatic segmentation of aortic computed tomography angiography combining multi-view 2d convolutional neural networks. Cardiovascular Engineering and Technology 2020; 11(5): 576-586.

Forcadel N., le Guyader C., Gout C. Generalized fast marching method: applications to image segmentation. Numerical Algorithms 2008; 48: 189-211.

MIC-DKFZ/MITK-Diffusion: MITK diffusion - Official part of the Medical Imaging Interaction Toolkit. https://github.com/MIC-DKFZ/MITK-Diffusion/ (Access date: 7.02.2023)

Hu J., Shen L., Sun G. Squeeze-and-excitation networks. In Proceedings of the IEEE Conference on Computer Vision And Pattern Recognition 2018: 7132-7141.

Jha D., Smedsrud PH., Riegler MA., Johansen D., De Lange T, Halvorsen P., Johansen HD. Resunet++: an advanced architecture for medical image segmentation. IEEE nternational symposium on multimedia (ISM) 9 Dec 2019: 225-2255.

Jin Q., Meng Z., Pham TD., Chen Q., Wei L., Su R. Dunet: a deformable network for retinal vessel segmentation. Knowledge-Based Systems 2018; 178:149-162.

Lareyre F., Adam C., Carrier M., Dommerc C., Mialhe C., Raffort J. A fully automated pipeline for mining abdominal aortic aneurysm using image segmentation. Scientific Reports 2019; 9(1): 1-14.

Lin P., Zheng C., Yang Y., Gu J. Medical image segmentation by level set method incorporating region and boundary statistical information. Lecture Notes in Computer Science 2004; 3287: 654-660.

Maolood IY., Al-Salhi YEA., Lu S. Thresholding for medical ımage segmentation for cancer using fuzzy entropy with level set algorithm. Open Medicine 2018; 13(1): 374-383.

Mendi AF. Edge ai technology in the defense industry via reinforcement learning in simulation environments. Gümüşhane Üniversitesi Fen Bilimleri Dergisi 2023;13(3): 718-732.

Morris ED., Ghanem AI., Dong M., Pantelic MV., Walker EM., Glide-Hurst CK. Cardiac substructure segmentation with deep learning for improved cardiac sparing. Medical Physics 2020; 47(2): 576-586.

Noothout JMH., de Vos BD., Wolterink JM., Isgum I. Automatic segmentation of thoracic aorta segments in low-dose chest ct. Published online October 9, 2018: 63.

Onthoni DD., Sheng TW., Sahoo PK., Wang LJ., Gupta P. Deep learning assisted localization of polycystic kidney on contrast-enhanced ct ımages. Diagnostics 2020; 10(12): 1113.

Otaki Y., Watanabe T., Konta T., et al. Impact of hyperuricemia on mortality related to aortic diseases: a 3.8-year nationwide community-based cohort study. Scientific Reports 2020; 10(1).

Pratondo A., Ong SH., Chui CK. Region growing for medical image segmentation using a modified multiple-seed approach on a multi-core cpu computer. IFMBE Proceedings 2014; 43: 112-115.

Radl L., Jin Y., Pepe A, Li J., Gsaxner C., Zhao FH., Egger J. Avt: multicenter aortic vessel tree cta dataset collection with ground truth segmentation masks. Data in Brief 2022; 40: 107801.

Ranjbarzadeh R., Bagherian KA., Jafarzadeh GS., Anari S., Naseri M., Bendechache M. Brain tumor segmentation based on deep learning and an attention mechanism using mrı multi-modalities brain images. Scientific Reports 2021; 11(1): 1-17.

Ronneberger O., Fischer P., Brox T. U-net: convolutional networks for biomedical image segmentation. Lecture Notes in Computer Science 2015; 9351: 234-241.

Szegedy C., Liu W., Jia Y., Sermanet P., Reed S., Anguelov D., Erhan D., Vanhoucke V., Rabinovich A. Going deeper with convolutions. In Proceedings of the IEEE Conference on Computer Vision and Pattern Recognition 2015: 1-9.

Ter-Sarkisov A. Lightweight model for the prediction of covıd-19 through the detection and segmentation of lesions in chest ct scans. MedRxiv 2020.

Urfali A., Celikten A., Bozkir OF., Demirel S., Budak A., Karataş H. Advanced kernelized google-net: a novel deep neural network for alzheimer's disease classification on mrı data (in press).

Wang HJ., Chen LW., Lee HY., Chung YJ., Lin YT., Lee YC., Chen YC., Chen CM., Lin MW. Automated 3d segmentation of the aorta and pulmonary artery on non-contrast-enhanced chest computed tomography ımages in lung cancer patients. Diagnostics 2022; 12(4): 967.

Yuan S, Yang F. Segmentation of aortic vessel tree in ct scans with deep fully convolutional networks. arXiv preprint arXiv:2305.09833. 2023.

Zheng JQ., Zhou XY., Li QB., Riga C., Yang GZ. Abdominal aortic aneurysm segmentation with a small number of training subjects. arXiv 2018.

Zhou B., Zhao H., Puig X., Fidler S., Barriuso A., Torralba A. Scene parsing through ade20k dataset. 2017 IEEE Conference on Computer Vision and Pattern Recognition (CVPR), 21-26 July 2017.